CARBON 50 (2012) 3753–3765

Available at www.sciencedirect.com

SciVerse ScienceDirect

journal homepage: www.elsevier.com/locate/carbon

Synthesis of nitrogen-doped porous graphitic carbons using nano-$CaCO_3$ as template, graphitization catalyst, and activating agent

*Guangwen Yang, Heyou Han *, Tingting Li, Chunyan Du*

State Key Laboratory of Agricultural Microbiology, College of Science, Huazhong Agricultural University, 1 Shizishan Street, Wuhan 430070, PR China

ARTICLE INFO

Article history:
Received 20 January 2012
Accepted 30 March 2012
Available online 9 April 2012

ABSTRACT

Nitrogen-doped porous graphitic carbons (NPGCs) with controlled structures were synthesized using cheap nano-$CaCO_3$ as template, melamine-formaldehyde resin as carbon precursor, and dilute HCl as template removing agent. In addition to its use as a template, the nano-$CaCO_3$ acted as an internal activating agent to produce micro- and mesopores, as an adsorbent to remove the released hazardous gases (i.e. HCN, NH_3), and as a mild graphitization catalyst. The obtained NPGCs with hierarchical nanopores contained as high as 20.9 wt% of nitrogen, had surface areas of up to 834 $m^2 g^{-1}$, and also exhibited high thermal stability with respect to oxidation. Using carbohydrate or phenolic resin as the carbon precursor, this simple approach was also capable of producing hierarchical porous graphitic carbons with high surface area (up to 1683 $m^2 g^{-1}$) and extremely large pore volumes (>6 $cm^3 g^{-1}$). X-ray diffraction and infrared spectroscopy suggested that the intermediate $CaCN_2$ or CaC_2 generated during the carbonization plays a critical role in the formation of the graphitic structure.

© 2012 Elsevier Ltd. All rights reserved.

1. Introduction

Nitrogen-doped carbons can be regarded as "noble carbons" because the incorporated nitrogen (N) atoms, even a small amount (<0.5%) [1], can largely improve the physicochemical properties of the carbons, such as conductivity, basicity, oxidation stability, and catalytic activity [2–8]. This is mainly believed to be due to the N lone-pair electrons can provide additional negative charges into the graphene π system and thus lead to an enhanced conducting behavior as well as a strong interaction with foreign molecules (i.e. acidic compounds, ions, metal particles) [9,10]. These properties are of significance for many challenging applications, including electronic and catalytic systems. Specially, in addition to its use as a high-performance catalyst support, N-doped carbon can find applications as a metal-free catalyst on its own both in organic synthesis and in fuel cell systems [8,11]. For example, the N-doped carbon exhibiting excellent electrocatalytic activity for oxygen-reduction reaction in fuel cells has recently been intensively investigated by research teams world-wide.

However, the higher amount of N incorporated in the carbon host alone does not always lead to better performance, which also crucially depends on its structural and morphological properties. It is generally recognized that the carbons with a moderate amount of N in the bulk, a graphite-like carbon structure, an optimized pore network/nanostructure, and/or a large surface area are highly favorable especially as the cathode catalyst for fuel cells; with such conditions that the materials being pursued will possess a higher conductivity, an improved chemical or electrochemical stability, a faster ion transport behavior, and a larger surface density of catalytic sites [4,6,12–15]. However, it is hard to synthesize this type of

* *Corresponding author:* Fax: +86 2787288246.
E-mail address: hyhan@mail.hzau.edu.cn (H. Han).
0008-6223/$ - see front matter © 2012 Elsevier Ltd. All rights reserved.
http://dx.doi.org/10.1016/j.carbon.2012.03.050

nanostructured carbons with both high N content and graphitization degree. This is because the graphitization process is generally occurred under very harsh conditions (>2000 °C) which would lead to the entirely elimination of N atoms, low yields, and/or nanostructural collapses [16]. So the search for new synthesis routes for the generation of N-doped graphitic carbons (NGCs) with controllable nanostructures has been an appealing topic in materials chemistry. Recently, the catalytic graphitization carried out with the aid of various transition-metal catalysts (i.e. Fe, Co, Ni, etc.), has been proven to be an effective means to prepare graphitic carbon with high crystallinity at relatively low temperatures. And thus NGCs can be prepared by the pyrolysis of transition-metal macrocyclic compounds or mixtures of metal salts and N-containing precursors, although some of which are rather expensive [14]. However, in most cases, the N content of the resulting carbon becomes quite low because the catalysts (i.e. Fe, Ni) with relatively high reactivity can simultaneously enhance the elimination of N at elevated temperatures [17–19]. Furthermore, in order to improve the surface area and nanostructure of the graphitic carbons, previous attempts mostly relies on the aid of hard-templating pathway using colloid or mesoporous silica, since direct pyrolysis of these precursors normally leads to bulk carbons with less (accessible) porosity [13,20]. But the involved silica template fabrication is often time-consuming, and in some cases, costly and usually includes the use of extremely toxic and corrosive reagents (i.e. HF) to remove these templates. It makes this method unpractical and to some extent limits their application in reality. Thus, the effective synthesis of novel N-doped porous graphitic carbons (NPGCs) from cheap and readily available raw materials under relatively mild conditions remains a challenging and important line of study in materials chemistry.

Triazines, especially melamines, with good stability and high N content have recently become remarkable units in the fabrication of N-doped carbon nanomaterials with graphitic structure [15,21,22]. For example, Wang et al. reported that carbon nanotubes with N-doping level as high as 20 atom% can be directly synthesized using melamine as C/N precursors through the detonation-assisted chemical vapor deposition method in a sealed vessel [15]. More recently, NGCs were prepared by thermolysis of task-specific ionic liquids containing abundant nitrile groups, in such a process that the triazine-based intermediates are formed by a trimerization of the nitrile groups. It was found that these intermediates showed a strong contribution to the high N content as well as the graphitic structure [3,4,23,24]. Thus, we believe that melamine-formaldehyde (MF) resin contains about 45 wt% of N and a substantial amount of triazine ring units would be also a promising candidate for the synthesis of NGC. Nevertheless, as far as we know, both the melamines and melamine resins are cheap and available triazine products used widely in the synthesis of porous N-rich materials (i.e. carbon nitrides and N-rich polymers) [25,26], they are seldom utilized as raw materials to prepare NGCs. One of the reason may be that carbonization of these resins will abundantly release an acute toxicant, hydrogen cyanide (HCN) in gas phase which are NO_X and N_2O precursors.

In contrast to the other vast number of nanostructured hard templates for the preparation of porous carbons, nano-$CaCO_3$ with unique mechanical/optical properties is rarely investigated, although it is one of the most abundant industrialized nanomaterials with cheap price (ca. $500/ton) [27]. At present, both the surface polarity and particle size of the nano-$CaCO_3$ can be well-tuned in industrial production, making it possible to meet the needs of various carbon precursors. Based on the above consideration, here, we proposed a simple protocol for the preparation of NPGCs with controllable shape at moderate temperatures by using MF resin as carbon precursor, nano-$CaCO_3$ as template, and diluted HCl instead of the corrosive HF acid for removing the template. Rather unexpected, the nano-$CaCO_3$ can simultaneously be severed as both a graphitization catalyst to form the highly graphitized structure and an adsorbent to reduce the release of hazardous gases (i.e. HCN, NH_3) by carbonization.

2. Experimental

2.1. Materials and synthesis

The NPGC was synthesized by copolymerization of melamine and formaldehyde in the presence of nano-$CaCO_3$ at controlled pH. Typically, 63 g of melamine (Tianjin Guangfu Fine Chemical Research Institute, 99.5%) was added to a 100 mL formaldehyde solution (Sinopharm Chemical Reagent Co., Ltd., 37% in water, stabilized by 8–14% methanol solution) under stirring, and the pH of the mixture was adjusted to 8–9 by adding diluted NaOH. The resulting milky solution was then heated to 80 °C for about 15 min to form a clear and colorless solution. After adjusting the solution to pH 5–6 by diluted HCl, varying amounts (50–120 g) of hydrophilic nano-$CaCO_3$ (Shanxi Xintai NanoMater. Co. Ltd., see Supporting information, Figs. S1 and 2) were added and thoroughly mixed into the solution with vigorous stirring. Depending on the amount of nano-$CaCO_3$, 0–30 mL H_2O was added to obtain a homogeneous solution. Over a 0.5–2 h period a gel-like mixture was prepared. Before complete solidification had occurred, we can mold the mixture to get monoliths. The composites were left to dry at 60 °C in air, and then slowly heated to 180 °C for overnight. Subsequently, for route A, the monoliths were directly carbonized at desired temperature for 2 h under N_2 flow, with a heating rate of 5 °C min^{-1}; while for route B, the monoliths were firstly ground to fine powders before the carbonization (Fig. 1). Finally, after etching the calcium templates by diluted HCl, the carbons were isolated, and dried under vacuum at 150 °C affording black powder as products.

Typical sample notation is as follows: MFA-*X*-*Y* or MFB-*X*-*Y* for the porous samples obtained from route A or B, respectively, where *X* stands for the amount of template added (0 g, 50 g, 70 g, 90 g, 100 g, 110 g, and 120 g correspond to *X* = 0–6, respectively) and *Y* stands for the temperature (°C) of carbonization (*Y* = 180–1300). Thus, the corresponding composite samples can be referred to MF/$CaCO_3$-*X*-*Y*.

For comparison, the carbons obtained from sucrose (Suc) and resorcinol-formaldehyde (RF) as carbon precursors are similarly called Suc-*X*-*Y* and RF-*X*-*Y*, respectively, of which the preparation methods are presented in Supporting information.

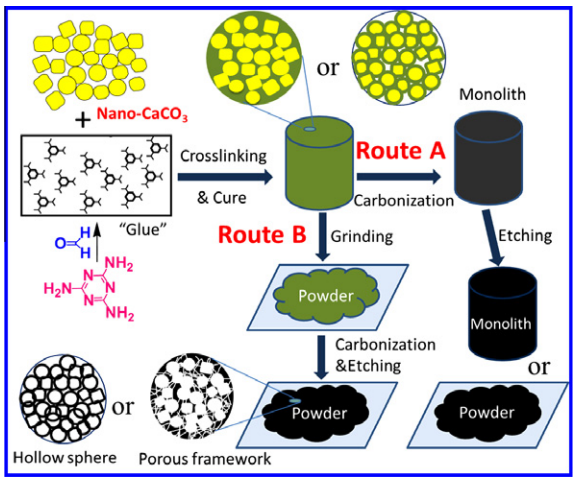

Fig. 1 – The synthesis route used to prepare NPGCs.

2.2. *Measurements and characterization*

Elemental analyses were performed on an Elementar Vario Micro-cube elemental analyzer. Scanning electron microscopy (SEM) images were taken by a JEOL JSM-6700F field emission scanning electron microscope. Transmission electron microscopy (TEM) images were recorded with a Hitachi H-7650 transmission electron microscope at an acceleration voltage of 120 kV. High-resolution TEM (HRTEM) images were taken by JEM-2010 with an accelerating voltage of 200 kV. Fourier transform infrared (FT-IR) spectra were collected on a Nicolet Avatar-330 spectrometer with 2 cm^{-1} resolution using the KBr pellet technique. Raman spectra were recorded by a Renishaw inVia Raman spectrometer equipped with a He–Ne laser excitation source operating at 632.8 nm. X-ray photoelectron spectra (XPS) were measured by a Thermo VG Multilab 2000 spectrometer equipped with a monochromatic Al Kα radiation source at room temperature. Binding energies for the high-resolution spectra were calibrated by setting C 1s at 284.6 eV. Thermal gravimetric analysis (TGA) measurements were examined using a NETZSH TG 209C thermobalance with a heating rate of 5 °C/min under N_2 (or 10 °C/min under air) and a flow rate of 20 cm^3/min. X-ray diffraction (XRD) measurement was performed on a Rigaku D/MAX-rA diffractometer with Cu Kα radiation ($\lambda = 1.5406$ Å). N_2 adsorption experiments and pore analysis were conducted at −196 °C using an Autosorb-1 from Quantachrome Instruments. Prior to the measurements, the samples were degassed in vacuum at 220 °C for 10 h. The total surface area was calculated from the Brunauer–Emmett–Teller (BET) equation from the adsorption data at relative pressures from 0.05 to 0.2. The pore size distribution (PSD) was determined by the Barrett–Joyner–Halenda (BJH) method using desorption data (for nanopores frameworks) or adsorption data (for hollow nanocages).

3. Results and discussion

3.1. *Synthesis of NPGC*

To obtain NPGC with high N content, N-rich MF resins had been used as carbon precursor in the presence of nano-$CaCO_3$ at controlled pH. The overall synthesis procedure used for NPGC is illustrated in Fig. 1. Firstly, melamine was dissolved in formaldehyde solution under basic conditions to obtain soluble, reactive methylol melamines as "glue", in which the $CaCO_3$ nanoparticles can be easily dispersed and stabilized because of the metal chelation interactions between $CaCO_3$ and MF resin, which was similar to the "col–gel" method published by Schmidt et al. [28] The propagation step in resin formation was the creation of methylene and ether linkages between the methylolated melamines upon further heating and acidifying the system, thus leading to the completely embedding of $CaCO_3$ template. To obtain the porous carbons, two synthesis routes were designed. For route A, before complete solidification had occurred, the gel-like mixtures were molded, and resulted in the formation of a rigid, white MF/$CaCO_3$ composite monolith following drying from aqueous media. After being cured at 180 °C inducing a higher degree of condensation, a yellow–brown monolith with some shrinkage was produced. With higher template amount (>70 g) and/or lower formaldehyde/melamine ratio, the monoliths were usually crack-free and can largely retain the original monolithic shape even after carbonization (Supporting information, Fig. S3). The cured monoliths were directly carbonized under N_2 atmosphere followed by or by not grinding into finely powder, yielding monolith or powdery samples, respectively. However, after the calcium template was dissolved in diluted HCl, stable porous carbon monoliths can only be obtained when the template was less than 80 g and the carbonized temperature was lower than 1000 °C (Fig. S4). For route B, the cured samples were firstly ground into powders before carbonization, and the other processes are similar to route A, yielding powder products (see Supporting information, Fig. S9).

As shown in Table 1, the carbon yield decrease first and then increase with the increase of carbonization temperatures. Particularly, the sample obtained at 900 °C (MFA-2-900) possesses the minimum carbon yield (18 wt%). The reasonable explanation will be given below.

3.2. *Morphology and microstructure observation*

The morphology and microstructure of several typical N-doped carbons prepared at different carbonized temperatures was studied by SEM and TEM (Fig. 2–4 and Supporting information, Figs. S5–24). For route A, the carbons prepared at 800 °C (MFA-2-800) have a well-developed pore system consisting of disordered, interconnected and roughly spherical pores mainly on the borderline between meso- and macropores, that is, 40–100 nm (Fig. 2a and b, and Supporting information, Fig. S5). It is in good agreement with the particle size distribution of nano-$CaCO_3$ (ca. 76 ± 30 nm, see Figs. S1 and 2). Similar pore structures can also be observed in the case of the samples prepared at 900–1100 °C (Fig. 3a, c, and e), although hollow nanocages can be occasionally detected for the case of MFA-2-1000 and -1100. It can be seen that the MFA-2-900 possess many mesopores with a diameter of about 10 nm at high magnification (Fig. 3a and Supporting information, Fig. S6), which for the MFA-2-800 shows a decrease in number; but it is almost invisible for the higher- or lower-temperature samples, especially for those prepared at 700 °C (Supporting information, Fig. S7). This is mainly attributed to the CO_2

Table 1 – Composition of samples MFA-2-Y (Y = 800–1300) and their carbon yields.

Samples	C[a]	N[a]	C/N[a,c]	C/N[b,c]	C/O[b]	N-Q/N-6[b]	Yield (wt%) [d]
MFA-2-800	62.3	20.9	2.6	3.9	6.2	0.8	23
MFA-2-900	70.7	10.9	5.6	8.5	7.2	1.8	18
MFA-2-1000	80.6	6.4	10.8	19.1	11.9	2.2	19
MFA-2-1100	86.0	3.6	20.5	46.2	16.2	4.3	21
MFA-2-1200	96.7	0.9	92.1	119.9	29.1	5.3	22
MFA-2-1300	96.9	0.6	138.4	137.4	31.0	–	21

[a] Derived from CHN elemental analysis.
[b] Derived from XPS.
[c] C/N and C/O refer to molar ratio.
[d] Yield is defined as: g carbon per 100 g cured MF resin.

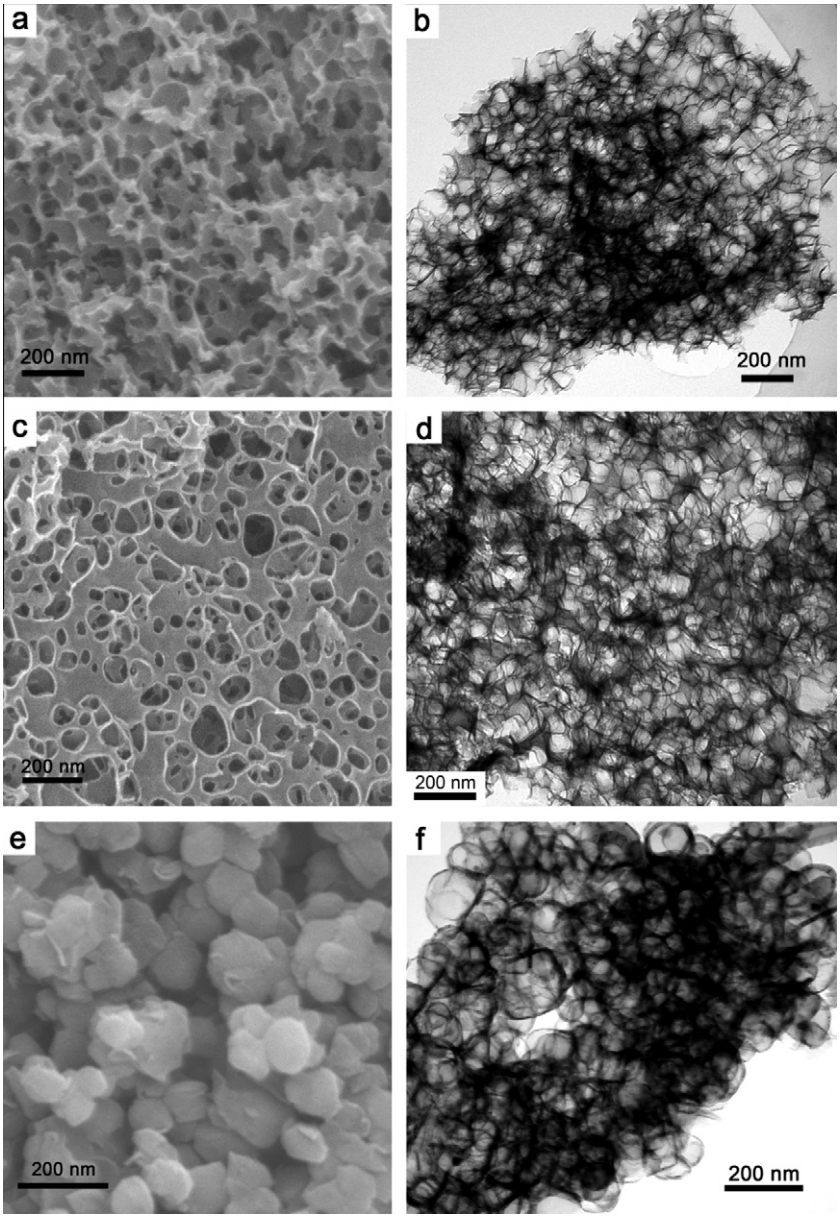

Fig. 2 – SEM and TEM images of the MFA-2-800 (a and b), MFB-2-800 (c and d), and MFB-2-1200 (e and f).

activation at above 700 °C and the gradual graphitization process at above 900 °C, which can be confirmed by the N_2 sorption and XRD analysis below. However, in the case of MFA-2-1200, aggregated hollow nanocage structures are

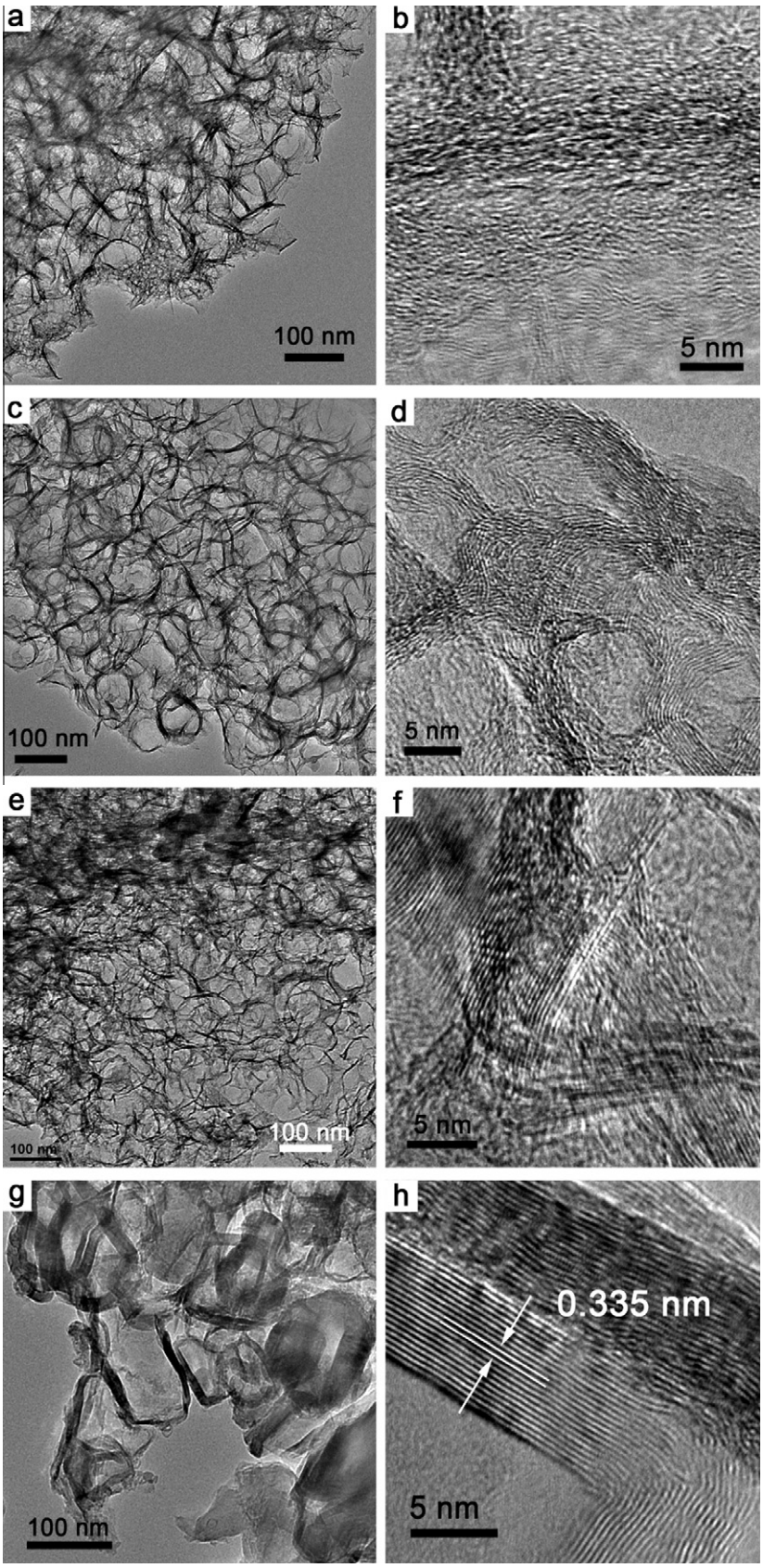

Fig. 3 – HRTEM images of samples MFA-2-Y, Y = 900 (a and b), 1000 (c and d), 1100 (e and f) and 1200 (g and h).

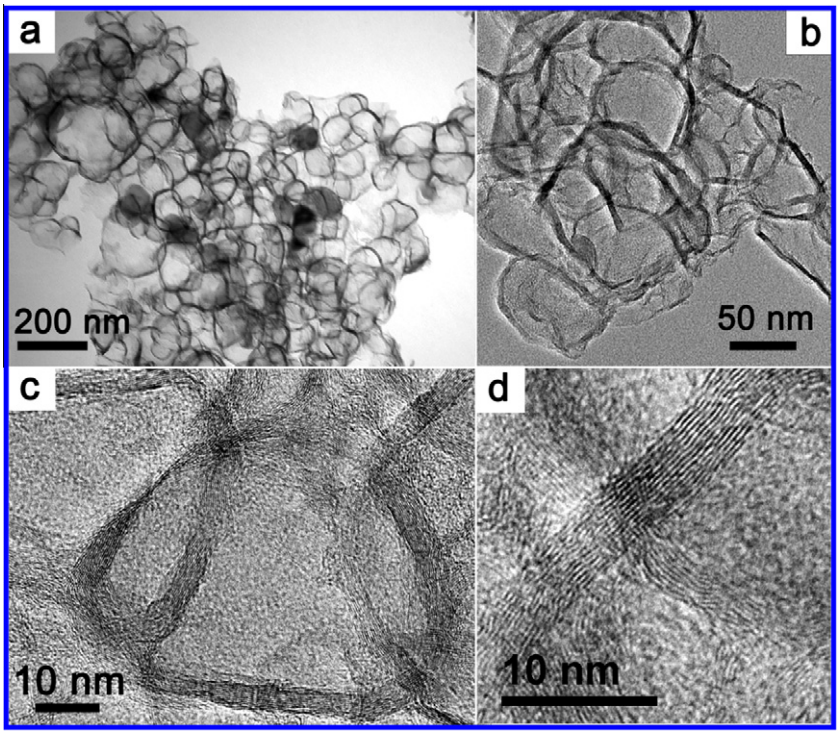

Fig. 4 – TEM (a and b) and HRTEM (c and d) images of MFB-3-1000.

observed (Fig. 3g and Supporting information, Fig. S8a). In most cases, the cage size is 40–120 nm with the shell thickness being 10–20 nm. Some of the cages have smaller-sized nanoparticles (10–40 nm) inside it. This indicates that some of the carbon shells are perfect maybe with dense packing of graphene layers and could to some extent protect the template cores from acid etching, which is further confirmed by the HRTEM images (Fig. 3h and Fig. S8b). It should be noted that many cages are not perfect in cage structure due to some fractures and defects, which may stem from structural collapses during the severe ground process before the template removal.

Shown in Fig. 3 (right panels) are the HRTEM images taken from the pore wall (or cage shell) of the samples carbonized at different temperatures (900–1200 °C). As seen in Fig. 3b, the MFA-2-900 shows a loosely stacking of curved graphene layers in the carbon matrix, suggesting the formation of graphitic microdomains, though the graphitization degree is rather low. For MFA-2-1000 (Fig. 3d), more obvious graphene layers which are packed tightly can be observed, indicating that carbonization at 1000 °C can largely improve the graphitization degree. The graphene layers are curved and interrupted, and have many defects. However, the MFA-2-1100 is made up of regularly rearranged graphene layers with a spacing of 0.34 nm, agreeing with the formation of relatively large graphite crystallities in the carbonaceous pore walls. A higher degree of long-range order is achieved by further increasing the temperature to 1200 °C, at such a temperature that the cage shells are composed of well-defined graphene layers with a spacing of 0.335 ± 0.003 nm. These graphene layers are parallel to the surface of the cage shell (Supporting information, Fig. S8b).

For route B, Fig. 2c and d depict, as an example, the electron micrographs of the corresponding samples carbonized at 800 °C (MFB-2-800). It can be seen that both the surface of the porous framework and the pore wall are well preserved (for more details see Supporting information, Figs. S10 and 11). Together with the case in route A, the observed well-developed three-dimensional (3D) system of pores throughout the carbon particles can thus be attributed to the complete filling of the entire void around the calcium template (volume templating) [29]. Each of the imperfect-spherical pores is also interconnected through small holes. More perfect nanocages can be obtained from this route at 1200 °C. It can be seen in Fig. 2e and f that the carbons survive as a series of agglomerates of carbon nanocages with about 50–120 nm in diameter and 10–15 nm in shell thickness (for more details see Supporting information, Fig. S12). Surprisingly, however, when the amount of template are 90 g or more, interconnected hollow nanocages with more homogenous shell thickness can be prepared at 1000 °C, that is, MFB-X-1000 (X = 3, 4, 5, 6) (see Fig. 4 and Supporting information, S13–16). The reason is probably due to the surface coating (surface templating) at these conditions with appropriate template amount and carbonization processes [29]. From the TEM images (Fig. 4 and Supporting information, Fig. S13), it is clear that the size of these hollow cages is mainly concentrated at 50–120 nm. The HRTEM images (Fig. 3b–d and Supporting information, Fig. S14) can support the TEM results and also reveal a well-defined graphitic shell with quite homogenous shell thickness (ca. 5 nm). While most cages appear to be closed, some show an open graphitic structure. Interestingly, some bamboo-like nanocages with high crystallinity can also be occasionally observed (Supporting information, Fig. S17), similar to the melamine-derived nanotubes in literature which is thought to be the result of rich nitrogen atoms were incorporated into the carbon networks [15].

Though the preparing methods, carbonization temperature and template amount can affect the morphologies to some extent. The results showed that the carbonized temperature is the most important factor to control the carbon structure. While at temperature below 1000 °C, nanoporous frameworks were obtained, at temperature of 1000 °C or higher, the resulting samples tend to form crystallized hollow nanocage. This may be due to the catalytic graphitization of the template at elevated temperatures and, in consequence, the graphitic shells are formed around the template nanoparticles, which can be further confirmed by the XRD analysis. Notably, the obtained nanoporous frameworks with a unique 3D interconnected meso- and macro-porous network, may make it easy for the fast transportation of large molecules and the large utilization of surface area, which are highly favorable for several important applications (e.g. large molecule separations, heterogeneous catalysis) [30]. And the presented carbon nanocages with tailored structural properties may find additional applications as advanced storage materials [31].

3.3. *Chemical structure*

In order to investigate in detail the temperature-dependent graphitic nature, we carried out XRD measurements for the porous carbons. As shown in Fig. 5, the peaks at around 26.2°, 42.5°, 44.4°, and 54.3° corresponds to the reflections of graphitic planes (0 0 2), (1 0 0), (1 0 1), and (0 0 4), respectively. They show an increase as the heating temperature increases, implying that the degree of graphitization depends positively on the temperature. Notably, at 1000 °C or higher, the resulting samples show a high-intensity sharp (0 0 2) signal along with clearly observable other (1 0 0), (1 0 1), and/or (0 0 4) reflections characteristic for 2D and 3D graphitic structures [32], exhibiting relatively high levels of graphitic character; and these bands are slightly upshifted by 0.7° from that of MFA-2-1000 (25.8°) to MFA-2-1300 (26.5°). However, at temperatures below 900 °C, only a weak broad (0 0 2) signal and no other reflections are observed, indicating that these samples are rather disordered; and the (0 0 2) band is downshifted by 1° from that of MFA-2-700 (26.8°) to MFA-2-1000 (25.8°), which is similar to the case observed in the literature [3]. Specially, although we do not observe obvious crystalline structures from the carbons derived from pure MF without templating at temperatures below 1000 °C, the produced carbon at temperatures above 1000 °C exhibits graphitic features to some extent (see Supporting information, Fig. S18a).These results indicate that the MF resins are a kind of precursors to generate graphitizable carbons, which are similar to the case using nitrile-containing ionic liquids as carbon precursors [3,23]. But it is impossible to form highly graphitized carbons at these temperatures without the use of graphitization catalyst.

Raman spectroscopy, a powerful tool for identifying structure, disorder, doping and the number of graphene layers of carbon materials, were then applied to characterize the carbon structure. As can be seen in Fig. 6a, the carbon samples heated to 1000 °C or lower show a lower-intensity G-band signal at 1590 cm^{-1} and a higher-intensity broad D-band at 1341 cm^{-1}, while the graphitized samples obtained at above 1000 °C exhibit a strong G-band signal at 1572 cm^{-1} and a lower-intensity D-band at 1328 cm^{-1}. The D-band is associated with the defects, curved sheets and dangling bonds in the carbon structures, while the G-band corresponds to the E 2 g mode of graphite. The reduced D/G-band intensity ratios, coupled with the decreased peak width (sharper line shape) with increasing temperature reflect a higher degree of graphitization at higher temperatures, consistent with the HRTEM and XRD results. Compared with commercial graphite powder (1578 cm^{-1}), test here, the G-bands of the current MF-based graphitic carbons downshift by 6 cm^{-1}, most probably caused by the N doping [33]. Notably, here we measure a pronounced, broad 2D-band at 2652 cm^{-1} in the sample heated to above 1000 °C, increasing in intensity as the heating temperature increases, while that of commercial graphite powder is located at 2663 cm^{-1}. This shape of 2D-band, combined with its downshifted peak position, is usually assigned to few layer graphene [33,34], confirming once again that the wall of the carbons, is very thin, maybe with a few graphitic layers. Compared with the nano-$CaCO_3$ templated carbons above, as expected, that of pure MF resins without templating

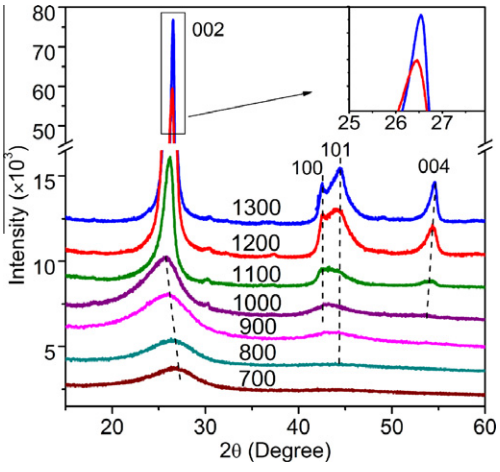

Fig. 5 – XRD patterns for samples MFA-2-Y (Y = 700–1300). Inset is the magnified view of the rectangular region.

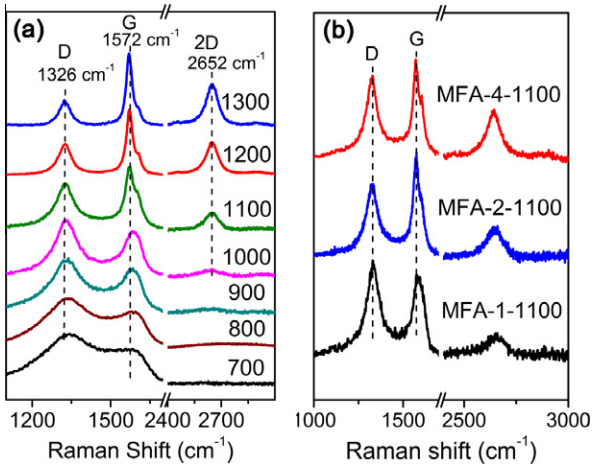

Fig. 6 – Raman spectra for samples (a) MFA-2-Y (Y = 700–1300) and (b) MFA-X-1100 (X = 1, 2, 4).

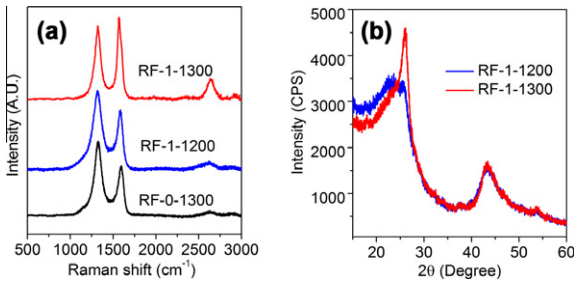

Fig. 7 – Raman spectra (a) and XRD patterns and (b) of the RF-based carbons.

carbonized at the same conditions show only two board, undivided peak at 1340 (D-band) and 1590 cm^{-1} (G-band), even at 1200 °C (Fig. S18b). Additionally, for a given carbonization temperature of 1100 °C, with increasing of the $CaCO_3$ ratio in the composite, the degree of graphitization increases distinctly. It can be deduced from the reduced D/G ratios in Raman spectra in Fig. 6b. Thus, based on the above results, it can be conclude that the calcium templates possess a good catalytic graphitization activity towards MF-based carbon, and this catalytic process is mainly occurred at 1000–1300 °C.

To evaluate the catalytic effect of this template for other carbon precursors, similar experiments using carbohydrate and phenolic resin as carbon precursors are performed. Fig. 7 shows the XRD and Raman profiles of the templated and untemplated carbons obtained from, as a typical example, RF resin at 1200–1300 °C. From the Raman spectra (Fig. 7a), it can be seen that the templated carbon RF-1-1300 has a lower relative intensity ratio ($I_D/I_G < 1$) and a more pronounced 2D peak than that of untemplated carbon RF-0-1300. In the XRD patterns (Fig. 7b), while the RF-1-1200 shows a board (0 0 2) peak at around 25°, the RF-1-1300 gives a complicated (0 0 2) pattern in which a broad profile has, superimposed over it, a sharp peak situated at 26°. Analogous results can also be observed in the case of carbohydrate (i.e. Suc, glucose, starch) derived carbons. For Suc as an example, the observed differences in the Raman and XRD profiles for both templated and untemplated carbons indicate that the calcium template has obvious catalytic activities for the graphitization of non-graphitizable carbons, especially at temperature of 1300 °C, though the graphitization degree is much lower than MF-based carbons (see Supporting information, Fig. S19). This means that the nano-$CaCO_3$ may be employed as a versatile catalyst to promote the formation of graphitic structures. According to Oya et al., the observed sharp peak at 26° (d_{002} = 0.342 nm) can be regard as *T* component, corresponding to the turbostratic structure, whereas the peak at 26.5° for MFA-2-1200 can be assigned to *G* component, corresponding to graphite structure [35,36]. These results can be further confirmed by the HRTEM observations (Fig. 8 and Supporting information, Figs. S20 and 21). It can be seen that both the Suc and RF derived carbons possess rather random stacking of curved graphene layers. However there are also many shell-like graphite ribbons with tightly, orderly packed graphene layers having interlayer spacing of 0.342 nm. This means that the formation of graphitic structures is easier to be occurred around the template nanoparticles, confirming once again the catalytic graphitization activity of the nano-$CaCO_3$.

3.4. *Composition analysis*

The compositions of samples MFA-2-Y (Y = 800–1300) are listed in Table 1. The data are the averages of two to four measurements. Elemental analysis (first three columns) shows that with increasing carbonization temperature from 800 to 1300 °C, the C content increases gradually from 62.3% (MFA-2-800) to 96.9% (MFA-2-1300), and in contrast, the N content decreases, that is, 20.9% (MFA-2-800), 10.9% (MFA-2-900), 6.4% (MFA-2-1000), 3.6% (MFA-2-1100), 0.9% (MFA-2-1200) and 0.6% (MFA-2-1300). Thus, the C/N molar ratio goes down to 2.6 for MFA-2-800 from 138.4 for MFA-2-1300. Particularly, these values of N content are comparable to or greater than the recently described porous MF-based carbons prepared at the similar carbonized conditions by SiO_2 [37,38], MgO [39], and mica [40] templating. That is to say, moderate amounts of N atoms could be retained in the carbons even when the heating temperature rising to 1100 °C (3.64%) in the presented carbonization process. Unlike the other carbons, however, the samples heated to above 1200 °C only show a rather low N content (<1%) and a high C content (>96%), suggesting that higher levels of graphitization are achieved at higher temperatures, nicely supporting the analysis results above. The same trends could also be observed from the results of XPS

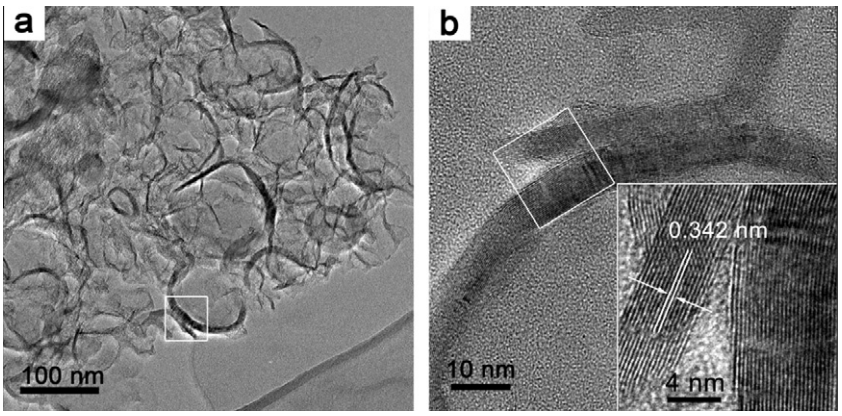

Fig. 8 – TEM (a) and HRTEM (b) images of the RF-1-1300. Inset is the magnified view of the rectangular region in (b).

analysis. Upon increasing temperatures from 800 to 1300 °C, the C/N molar ratio derived from XPS data is increased gradually from 3.9 to 137.4, and the molar ratio of C/O increases similarly from 6.2 to 31.0. This further demonstrates that the non-C elements (N and O) are highly unstable at higher temperatures, especially for the graphitization process (>1000 °C) [6]. It can also be observed that the C/N molar ratios from elemental analysis for all samples synthesized are generally lower than those from XPS analysis. It reveals that the amounts of the surface N are possibly less than the ones in the bulk materials, coinciding with the literature data concerning melamine-based carbon [6,41]. Surprisingly, the apparent oxygen content is fairly high, and a similar level of the oxygen is observed in the melamine-based carbons reported previously [37,39].

XPS spectra can additionally reveal the surface binding states and elemental speciation on the surface. No obvious peaks from Ca 2p (Ca: <0.4% atomic) were observed, implying that the calcium template was nearly or completely removed by treatment in diluted HCl, or totally encapsulated by the carbon shell, if any more. Shown in Fig. S22 (Supporting information) are N 1 s peaks of the samples MFA-2-Y (Y = 800–1300). The fitting of the N 1 s peak situated at about 399 eV for MFA-2-800 (Fig. S22a) indicates the presence of pyridine (N-6; 398.5 ± 0.3 eV; 42.3% area), pyrrole (N-5; 400.2 ± 0.3 eV; 21.0% area), quatenary (N-Q; 401.2 ± 0.3 eV; 31.7% area) and oxidized (N-O, 403.6 eV, 5.0% area) N, demonstrating the incorporation of N into the bulk aromatic carbon structure with pyrrolic-type systems dominating at this temperature. Upon further increasing carbonization temperature, peaks which can be attributed to N-5 and N-6 are gradually attenuated in the N1s spectra and finally absent at the temperatures of 1100 and 1300 °C, respectively; while that of N-Q becomes stronger and stronger (all the spectra are normalized with respect to the peak height). As expected, with temperature rising from 800 to 1200 °C, the ratio of N-Q/N-6 increases gradually, that is, from 0.8 for MFA-2-800 to 5.3 for MFA-2-1200. Thus, it can be conclude that the order of stability of the three types of N atoms is N-Q > N-6 > N-5, agreeing well with the literature [6,42].

3.5. *Thermal behavior*

Shown in Fig. S23a in Supporting information are the TG curves of samples MFA-2-Y (Y = 800–1300) under oxygen. It clearly reveals that the calcium templates can easily be removed by diluted HCl (residual weight below 4 wt%). The temperature range of main weight loss is observed to be between 450 and 706 °C for MFA-2-800, between 515 and 638 °C for MFA-2-900, between 543 and 685 °C for MFA-2-1000, between 594 and 746 °C for MFA-2-1100, between 621 and 760 °C for MFA-2-1200, and between 636 and 768 °C for MFA-2-1300. As already reported by Su et al., the oxidation reaction of carbon materials first occurs on the graphene layer edge defects or disordered graphene layers. In general, a higher oxidation temperature indicates higher thermal stability, and thus a higher graphitic extent. The sequence of oxidation temperature range of the carbons in air, here, follows the graphitization degree as provided by the HRTEM, XRD and Raman data, agreeing well with the literature [43,44]. Notably, the Suc and RF derived carbons also exhibit a comparable oxidation stability compared with that of the MF-based graphitic carbons above, that is between 627 and 721 °C and 650–760 °C for Suc-1-1300 and RF-1-1300, respectively (Supporting information, Fig. S24). This is mainly because of these carbons with turbostratic structure which are also known to be highly stable [35], similar to the case for carbon black.

3.6. *Pore structure analysis*

The nanometer structure of the pore system was additionally characterized by N_2 sorption measurements. All the N_2 sorption isotherms appeared very similar, with the exception of the carbons with hollow nanocage structure. Fig. 9 shows, as typical examples, the N_2 sorption isotherms and the corresponding PSDs of the as-synthesized carbons (for more details see Supporting Information, Figs. S25–34). As seen in Fig. 9a, the isotherms for the porous carbon frameworks are of type II with associated H3 type hysteresis loop, reflecting the macroporous and/or large-mesoporous nature, although micropores are also present [44,45]; and the corresponding PSD indicates that the pore size is centered largely in the range of 30–150 nm (inset), going well with the SEM and TEM results presented before. The sorption isotherms from route B are similar to that of route A, but the BET surface area (S_{BET}) from route B is lower than that of route A (327 $m^2 g^{-1}$ for MFA-2-800 and 295 $m^2 g^{-1}$ for MFB-2-800). As shown in Table 2, the S_{BET} and pore volume of MFA-2-Y (Y = 700–1300)

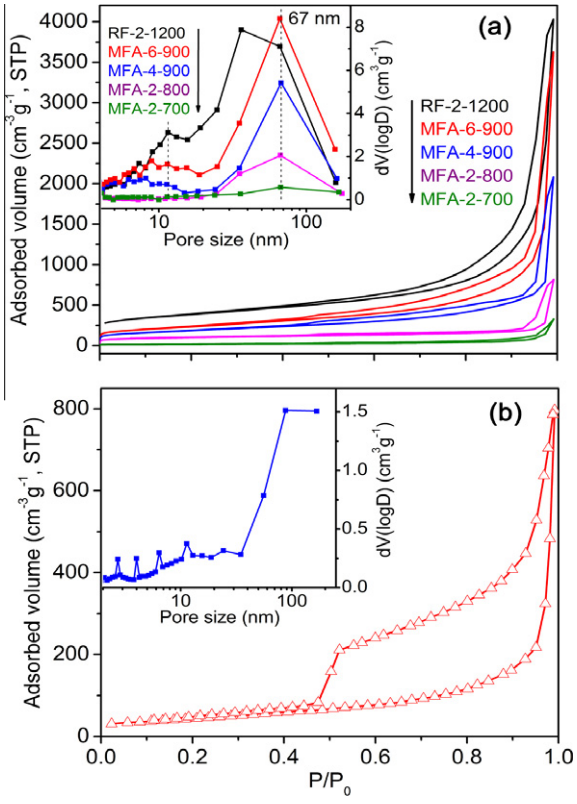

Fig. 9 – Typical N_2 sorption isotherms of the resultant nanoporous carbon framework (a) and hollow carbon nanocage (b, MFB-4-1000), together with their corresponding BJH PSDs (inset).

Table 2 – Textural parameters determined for the MF-, Suc-, and RF-based carbons.

Samples	$CaCO_3$ amount (g)	S_{BET} ($m^2\ g^{-1}$)[a]	V_{total} ($cm^3\ g^{-1}$)[b]	V_{micro} ($cm^3\ g^{-1}$)[c]
MFA-2-700	70	90	0.50	0.03
MFA-2-800	70	327	1.27	0.14
MFB-2-800	70	295	1.06	0.11
MFA-2-900	70	446	1.81	0.16
MFA-4-900	100	658	3.23	0.25
MFA-6-900	120	834	5.64	0.31
MFA-2-1000	70	196	1.75	0.073
MFB-3-1000	90	220	1.98	0.082
MFB-4-1000	100	160	1.24	0.057
MFB-6-1000	120	138	1.21	0.050
MFA-2-1100	70	175	1.34	0.064
MFA-2-1200	70	84	0.51	0.022
MFA-2-1300	70	51	0.40	0.015
Suc-1-1200	30	1301	4.95	0.50
Suc-2-1200	60	1683	6.67	0.53
Suc-1-1300	30	1217	4.71	0.48
RF-2-1200	60	1346	6.25	0.63
RF-2-1300	60	1262	6.14	0.48

[a] BET surface area.
[b] Pore volume calculated from N_2 adsorption at $p/p^0 \approx 0.99$.
[c] Micropore volume calculated from N_2 adsorption at $p/p^0 \approx 0.1$.

increases first and then decrease with increasing carbonized temperature. While only limited surface area ($S_{BET} < 100\ m^2\ g^{-1}$) were obtained for the samples carbonized below 700 °C, in the case of carbons prepared at 800 and 900 °C, the S_{BET} increases sharply up to 327 and 416 $m^2\ g^{-1}$, respectively; this can be attributed to the "CO_2 inner-activation effect" of the nano-$CaCO_3$ at 800–900 °C, producing more micro- and meso-pores [45]. The increased micropore can be proved by the increased N_2 uptake at low relative pressures, whereas mesopore can be verified by the TEM images of which the MFA-2-700 shows no observable small mesopore (Supporting information, Fig. S7). Yet when the carbonization temperature exceeds 900 °C, the S_{BET} decreases remarkably with increasing heating temperature, that is, ranging from 220 $m^2\ g^{-1}$ for MFA-2-1000 to 51 $m^2\ g^{-1}$ for MFA-2-1300; which can be mainly attributed to the decline of the micro- and/or meso-pores because of the gradual graphitization of the pore wall leading to a more dense packing of ordered graphene layers. Notably, for a given carbonized temperature at 900 °C, the S_{BET} of the carbon increases greatly with increasing the $CaCO_3$ amount in the $CaCO_3$/MF composites. Specially, the highest surface area (834 $m^2\ g\ g^{-1}$) and porous volume (5.6 $cm^3\ g^{-1}$) is obtained in the case of MFA-6-900; but it is much lower than that of Suc (1683 $m^2\ g^{-1}$; 6.7 $cm^3\ g^{-1}$) and RF- (1346 $m^2\ g^{-1}$; 6.3 $cm^3\ g^{-1}$) derived carbons produced here, which show a more broad PSD containing large numbers of mesopores (less than 20 nm), consistent well with the TEM observation. These values of surface area are much higher than that of ~50 nm nano-$CaCO_3$ templated carbons prepared at temperatures below 1000 °C, and comparable to that of 24 nm colloidal silica template amorphous carbons [27,45,46]. It is worthy to note that these isotherms for RF- and Suc-based carbon show an extremely high N_2 uptake (>4000 $cm^3\ g^{-1}$), which corresponds to >6.0 $cm^3\ g^{-1}$ total pore volume, much higher than many commonly silica templated carbons [3,4,29,32,46].

On the other hand, however, unlike the samples with porous frameworks above, ink-bottle-type IV N_2 sorption profiles with obvious hysteresis of desorption are observed for the samples with nanocage structures. Fig. 9b depicts, as an example, the sorption isotherm for selected sample MFB-4-1000 (for more details see Supporting information, Figs. S27 and 28), further confirming that these samples are indeed of hollow nanocage morphology with porous wall rather than porous framework [47]. The BJH PSD exhibits a broad distribution, that is 40–150 nm (Fig. 9b, inset), agreeing well with the results derived from TEM measurements.

4. Graphitization mechanism

3D nanostructured graphitic carbons (i.e. nanoporous frameworks, hollow nanocages) can be prepared using nano-$CaCO_3$ as both template and graphitic catalyst at relatively low carbonized temperature. It makes our investigation significant since both nano-$CaCO_3$ and the carbon precursors used are cheap and readily available industrialized chemicals. To the best of our knowledge, the current synthesis approach is the first example using $CaCO_3$ not only as a template but also as a graphitization catalyst to prepare nanostructured graphitic carbons at relative low temperature by such a simple route. Therefore, understanding how the graphitization forms is important in preparing more functional carbon materials. Though several calcium compounds have yet been reported to be as graphitization catalyst at high temperatures (>1800 °C) in 1970s, the information about the graphitization mechanism is still very sparse [35,36,48]; and thus nearly nothing is known about the mechanism leading to graphitized carbon in this carbonization system. To learn about the kinetic details of the formation of this unusual structure, the temperature-dependent structural evolution of graphitic carbon from MF was investigated by TGA, FT-IR, and XRD.

Clearly, the demonstration on the reaction behavior of $CaCO_3$ is helpful in comprehending how calcium template affects the carbonization and graphitization process. A series of specimen were collected from the same batch of the $CaCO_3$/MF composite samples before and after the pyrolysis. Fig. 10 shows how the XRD patterns of composite samples vary as a function of temperature. When the pyrolysis temperature is below 400 °C, it exhibits negligible effects on the XRD patterns, indicating that the nano-$CaCO_3$ in the composite is stable at these temperatures. When the temperature exceeds 400 °C, the diffraction peaks for calcium cyanamide ($CaCN_2$) phase appears, indicating that some of $CaCO_3$ begin to react with N-compounds (i.e. NH_3, HCN) provided by the thermal decomposition of MF maybe through the gas–solid reactions (1) and (2), in which the T_p stands for the temperature, and thus the $CaCN_2$ phase is generated.

$400\ ^\circ C < T_p \leqslant 700\ ^\circ C$

$$CaCO_3 + 2HCN \rightarrow CaCN_2 + CO + H_2 + CO_2 \quad (1)$$

$$CaCO_3 + 2NH_3 \rightarrow CaCN_2 + 3H_2O \quad (2)$$

When the temperature rises to 800 °C, the diffraction peaks belonging to $CaCO_3$ disappear and those for $CaCN_2$ phase become strongest, leading to a highest content of $CaCN_2$ in the sample. In view of the decomposition of $CaCO_3$ at around 720 °C (see reaction (3)), the reactions (4), (5) and (6) are involved [49,50]. The reaction (6) is the mechanism of the CO_2 activation, and it also explains why the carbon yield decreases (Table 1) and the S_{BET} increases (Table 2) with the carbonized temperature increased from 700 to 900 °C. Therefore, the formed meso- and micro-pores for MFA-2-Y (Y = 800–900) can also be well understood.

$700\ ^\circ C < T_p \leqslant 900\ ^\circ C$

$$CaCO_3 \rightarrow CaO + CO_2 \quad (3)$$

$$CaO + 2HCN \rightarrow CaCN_2 + CO + H_2 \quad (4)$$

$$CaO + 2CO + 2NH_3 \rightarrow CaCN_2 + CO_2 + 3H_2 \quad (5)$$

$$CO_2 + C \rightarrow 2CO(CO_2\ \text{activation}) \quad (6)$$

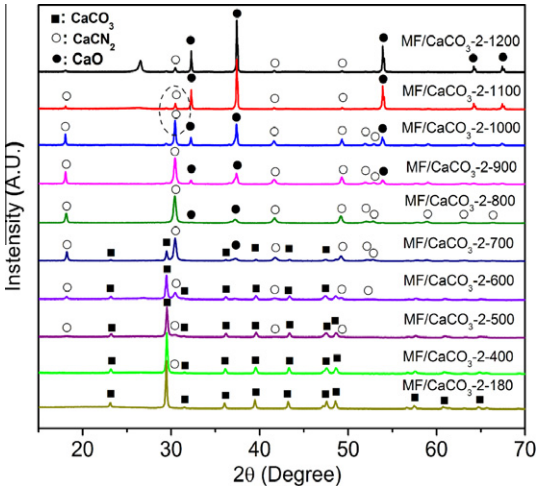

Fig. 10 – XRD patterns for composite samples MF/$CaCO_3$-2-Y (Y = 180–1200).

$$CaCN_2 + 3H_2O \rightarrow CaO + CO_2 + 2NH_3 \quad (7)$$

It is well known that both the HCN and NH_3 are hazardous gases, especially for HCN, an acute toxicant. Thus, the current carbonization process may be a promising method for in situ removal of the poisonous gas caused by the pyrolysis of N-containing carbon precursors. In fact, heating calcium-based materials in the presence of N-containing species (HCN, NH_3, etc.) has ever been an efficient method to produce $CaCN_2$, and recently becomes a novel hot gas cleanup method to capture these gases from coal gasification products [49,50]. However, with further increasing temperature, the diffractions attributed to CaO phase which began to appear at 700 °C gradually increase, while the diffractions assigned to $CaCN_2$ decrease. This indicates that $CaCN_2$ is converted to CaO, may be through the reaction (7), in which the H_2O is formed by the simultaneously elimination of O and H atoms [51]. However, at the temperature above 1000 °C, this contribution is very small because there are no enough O and H atoms.

According to literatures [51,52], the $CaCN_2$ can react with carbon at above 1000 °C to form unstable $Ca(CN)_2$ through the reaction (8), and then the decomposition reaction (9) occurs, where the A component corresponds to the amorphous carbon. In nanoparticle form, the decomposition results in phase separation to generate a $CaCN_2$ core surrounded by a carbon shell with well-crystallized structure [53], agreeing well with the HRTEM observations. Thus, the carbons obtained at 1200 °C with much thicker shell can be well understood. Specially, when the sample was heated up to 1100 °C, the diffractions assigned to $CaCN_2$ are dramatically attenuated, indicating a sharp decrease of the $CaCN_2$ in the sample. This is because the decomposition of $CaCN_2$ at above 1100 °C through the reaction (10), leading also to the formation of crystallized carbon structures. This is why the carbon yields increase with raising the temperature from 1000 to 1100 °C and have little change at elevated temperatures, as clearly shown in Table 1.

$T_p \geqslant 1000\ ^\circ C$ (Graphitization)

$$CaCN_2 + C\ (A\ \text{component}) \rightarrow Ca(CN)_2\ (\text{slow}) \quad (8)$$

$$Ca(CN)_2 \rightarrow CaCN_2 + C\ (G\ \text{component})(\text{fast}) \quad (9)$$

$$CaCN_2 \rightarrow Ca + C\ (\text{Gcomponent}) + N_2\ (> 1100\ ^\circ C) \quad (10)$$

That is to say, the in situ formed $CaCN_2$ can also be regard as an additional carbon precursor at higher temperatures (>1100 °C). Taking into consideration the finite size effect of the calcium-containing nanoparticles, all the reaction may be occurred at much lower temperatures. Surprisingly, however, neither $Ca(CN)_2$ nor metallic Ca are observed in the XRD profile for all the samples. Considering that the higher amounts of CaO in higher- temperature composite samples, the recorded CaO is supported to be formed during the process of taking out the sample from the furnace, because both Ca and $Ca(CN)_2$ nanoparticles are quite active in air (see the reactions (11) and (12)) [51].

$$Ca(CN)_2 + 3H_2O \rightarrow CaO + 2NH_3 + 2CO \quad (11)$$

$$2Ca + O_2 \rightarrow 2CaO \quad (12)$$

The TGA and FT-IR data can nicely support the XRD results and achieve a more detailed understanding about both the

carbonization and graphitization processes (see Supporting information, Figs. S23b, 35, and 36 and their analysis results).

For carbohydrate and phenolic resin derived carbon, there is no $CaCN_2$ be detected from the XRD patterns of the composite sample even at 1300 °C, suggesting that the graphitization mechanism for the non-N-containing carbon precursors is rather different from that of MF based carbon (Supporting information, Fig. S37). The most possible formation mechanism is shown in reactions (13) and (14), in which the unstable intermediate CaC_2 is the important chemical to form the *T* component instead of G component. This may result from the finely dispersion of the catalyst nanoparticle as well as the relatively low carbonization temperatures than the literature (>1800 °C) [48]. However, the reaction (13) is normally occurred at temperature above 1600 °C and the obtained results, here, may be stem from the finite size effect of the CaO nanoparticle. The graphitic shell-like structures created by the dissolution of template nanoparticles provides further evidence of this mechanism, similar to the case in literature [53].

$$CaO + 3C\ (A\ component) \rightarrow CaC_2 + CO \quad (13)$$

$$CaC_2 + CO \rightarrow CaO + 3C\ (T\ component) \quad (14)$$

5. Summary

We have presented an easy route to synthesize NPGCs using MF resin as carbon precursor and nano-$CaCO_3$ as template at moderate temperatures (⩽1300 °C). Several unique characteristics make the materials promising candidates for potential applications in material science: (i) because of the use of nano-$CaCO_3$ as template, this method does not require other graphitization catalyst and activation processes, and can reduce the release of hazardous gases, which simplifies operations and reduces the cost; (ii) as a novel graphitization catalyst, the nano-$CaCO_3$ is one of the most abundant and cheapest nano-sized materials; (iii) the obtained NPGCs with controlled structures contained as high as 20.9 wt% of nitrogen, had surface areas of up to 834 $m^2 g^{-1}$, and also exhibited high thermal stability with respect to oxidation, which may open a wide door for its applications especially in catalysis, supercapacitors, and full cell systems.

More importantly, this simple route is also capable of producing 3D hierarchical porous graphitic carbons with high surface areas (as high as 1683 $m^2 g^{-1}$) and extremely large pore volumes (>6 $cm^3 g^{-1}$) using non-N-containing carbon precursor (i.e. phenolic resin, carbohydrate). The $Ca(CN)_2$ or CaC_2 generated during the carbonization plays a critical role in the formation of graphitized structure. We believe this synthesis route will not only pave a new way for the preparation of NGCs but also for mass production of high-quality nanostructured graphitic carbons, since much more carbons can be directly obtained by the current method.

Acknowledgments

The authors gratefully acknowledge the support for this research by National Natural Science Foundation of China (20975042, 21175051), the Fundamental Research Funds for the Central Universities (2010PY009, 2011PY139), and the Natural Science Foundation of Hubei Province Innovation Team (2011CDA115).

Appendix A. Supplementary data

Additional experimental information, photos, TEM and SEM images, XPS data, TGA profile, FT-IR and Raman spectra, N_2 adsorption data, and XRD patterns and some results as noted in the text.

Supplementary data associated with this article can be found, in the online version, at http://dx.doi.org/10.1016/j.carbon.2012.03.050.

REFERENCES

[1] Latil S, Roche S, Mayou D, Charlier J-C. Mesoscopic transport in chemically doped carbon nanotubes. Phys Rev Lett 2004;92(25):256805–8.
[2] Gong K, Du F, Xia Z, Durstock M, Dai L. Nitrogen-doped carbon nanotube arrays with high electrocatalytic activity for oxygen reduction. Science 2009;323(5915):760–4.
[3] Paraknowitsch JP, Zhang J, Su D, Thomas A, Antonietti M. Ionic liquids as precursors for nitrogen-doped graphitic carbon. Adv Mater 2010;22(1):87–92.
[4] Yang W, Fellinger T-P, Antonietti M. Efficient metal-free oxygen reduction in alkaline medium on high-surface-area mesoporous nitrogen-doped carbons made from ionic liquids and nucleobases. J Am Chem Soc 2010;133(2):206–9.
[5] Jeong HM, Lee JW, Shin WH, Choi YJ, Shin HJ, Kang JK, et al. Nitrogen-doped graphene for high-performance ultracapacitors and the importance of nitrogen-doped sites at basal planes. Nano Lett 2011;11(6):2472–7.
[6] Su F, Poh CK, Chen JS, Xu G, Wang D, Li Q, et al. Nitrogen-containing microporous carbon nanospheres with improved capacitive properties. Energy Environ Sci 2010;4:717–24.
[7] Hulicova-Jurcakova D, Kodama M, Shiraishi S, Hatori H, Zhu ZH, Lu GQ. Nitrogen-enriched nonporous carbon electrodes with extraordinary supercapacitance. Adv Funct Mater 2009;19(11):1800–9.
[8] Yu D, Nagelli E, Du F, Dai L. Metal-free carbon nanomaterials become more active than metal catalysts and last longer. J Phys Chem Lett 2010;1(14):2165–73.
[9] Zhou Y, Neyerlin K, Olson TS, Pylypenko S, Bult J, Dinh HN, et al. Enhancement of Pt and Pt-alloy fuel cell catalyst activity and durability via nitrogen-modified carbon supports. Energy Environ Sci 2010;10(3):1437–46.
[10] Shao Y, Sui J, Yin G, Gao Y. Nitrogen-doped carbon nanostructures and their composites as catalytic materials for proton exchange membrane fuel cell. Appl Catal B: Environ 2008;79(1):89–99.
[11] Figueiredo JL, Pereira MFR. The role of surface chemistry in catalysis with carbons. Catal Today 2010;150(1–2):2–7.
[12] Yang X, Wu D, Chen X, Fu R. Nitrogen-enriched nanocarbons with a 3-D continuous mesopore structure from polyacrylonitrile for supercapacitor application. J Phys Chem C 2010;114(18):8581–6.
[13] Sevilla M, Fuertes AB. Catalytic graphitization of templated mesoporous carbons. Carbon 2006;44(3):468–74.
[14] Liu R, Wu D, Feng X, Müllen K. Nitrogen-doped ordered mesoporous graphitic arrays with high electrocatalytic activity for oxygen reduction. Angew Chem Int Ed 2010;49(14):2565–9.

[15] Wang Z, Jia R, Zheng J, Zhao J, Li L, Song J, et al. Nitrogen-promoted self-assembly of N-doped carbon nanotubes and their intrinsic catalysis for oxygen reduction in fuel cells. ACS Nano 2011;5(3):1677–84.
[16] Gierszal KP, Jaroniec M, Kim T-W, Kim J, Ryoo R. High temperature treatment of ordered mesoporous carbons prepared by using various carbon precursors and ordered mesoporous silica templates. New J Chem 2008;32(6):981–93.
[17] Nabae Y, Moriya S, Matsubayashi K, Lyth SM, Malon M, Wu L, et al. The role of Fe species in the pyrolysis of Fe phthalocyanine and phenolic resin for preparation of carbon-based cathode catalysts. Carbon 2010;48(9):2613–24.
[18] Yuan J, Giordano C, Antonietti M. Ionic liquid monomers and polymers as precursors of highly conductive, mesoporous, graphitic carbon nanostructures. Chem Mater 2010;22(17):5003–12.
[19] Watanabe T, Ohtsuka Y, Nishiyama Y. Nitrogen removal and carbonization of polyacrylonitrile with ultrafine metal particles at low temperatures. Carbon 1994;32(2):329–34.
[20] Fuertes AB, Alvarez S. Graphitic mesoporous carbons synthesised through mesostructured silica templates. Carbon 2004;42(15):3049–55.
[21] Terrones M, Terrones H, Grobert N, Hsu WK, Zhu YQ, Hare JP, et al. Efficient route to large arrays of CN_x nanofibers by pyrolysis of ferrocene/melamine mixtures. Appl Phys Lett 1999;75(25):3932–4.
[22] Sun Z, Yan Z, Yao J, Beitler E, Zhu Y, Tour JM. Growth of graphene from solid carbon sources. Nature 2010;468(7323):549–52.
[23] Lee JS, Wang X, Luo H, Dai S. Fluidic carbon precursors for formation of functional carbon under ambient pressure based on ionic liquids. Adv Mater 2009;22(9):1004–7.
[24] Lee JS, Wang X, Luo H, Baker GA, Dai S. Facile ionothermal synthesis of microporous and mesoporous carbons from task specific ionic liquids. J Am Chem Soc 2009;131(13):4596–7.
[25] Jurgens B, Irran E, Senker J, Kroll P, Muller H, Schnick W. Melem (2,5,8-triamino-tri-s-triazine), an important intermediate during condensation of melamine rings to graphitic carbon nitride: synthesis, structure determination by X-ray powder diffractometry, solid-state NMR, and theoretical studies. J Am Chem Soc 2003;125(34):10288–300.
[26] Yang G, Han H, Du C, Luo Z, Wang Y. Facile synthesis of melamine-based porous polymer networks and their application for removal of aqueous mercury ions. Polymer 2010;51(26):6193–202.
[27] Xu B, Peng L, Wang G, Cao G, Wu F. Easy synthesis of mesoporous carbon using nano-$CaCO_3$ as template. Carbon 2010;48(8):2377–80.
[28] Schmidt DF, Du Fresne von Hohenesche C, Weiss A, Schädler V. Colloidal gelation as a general approach to the production of porous materials. Chem Mater 2008;20(9):2851–3.
[29] Yu J-S, Kang S, Yoon SB, Chai G. Fabrication of ordered uniform porous carbon networks and their application to a catalyst supporter. J Am Chem Soc 2002;124(32):9382–3.
[30] Wang DW, Li F, Liu M, Lu GQ, Cheng H-M. 3D aperiodic hierarchical porous graphitic carbon material for high-rate electrochemical capacitive energy storage. Angew Chem 2008;120(2):379–82.
[31] Li Y, Zhou C, Xie X, Shi G, Qu L. Spontaneous, catalyst-free formation of nitrogen-doped graphitic carbon nanocages. Carbon 2010;48(14):4190–6.
[32] Yoon SB, Chai GS, Kang SK, Yu J-S, Gierszal KP, Jaroniec M. Graphitized pitch-sased carbons with ordered nanopores synthesized by using colloidal crystals as templates. J Am Chem Soc 2005;127(12):4188–9.
[33] Wei D, Liu Y, Wang Y, Zhang H, Huang L, Yu G. Synthesis of N-doped graphene by chemical vapor deposition and its electrical properties. Nano Lett 2009;9(5):1752–8.
[34] Ferrari AC, Meyer JC, Scardaci V, Casiraghi C, Lazzeri M, Mauri F, et al. Raman spectrum of graphene and graphene layers. Phys Rev Lett 2006;97(18):187401–4.
[35] Oya A, Otani S. Influences of particle size of metal on catalytic graphitization of non-graphitizing carbons. Carbon 1981;19(5):391–400.
[36] Oya A, Otani S. Catalytic graphitization of carbons by various metals. Carbon 1979;17(2):131–7.
[37] Li W, Chen D, Li Z, Shi Y, Wan Y, Huang J, et al. Nitrogen enriched mesoporous carbon spheres obtained by a facile method and its application for electrochemical capacitor. Electrochem Commun 2007;9(4):569–73.
[38] Pevida C, Drage TC, Snape CE. Silica-templated melamine-formaldehyde resin derived adsorbents for CO_2 capture. Carbon 2008;46(11):1464–74.
[39] Konno H, Onishi H, Yoshizawa N, Azumi K. MgO-templated nitrogen-containing carbons derived from different organic compounds for capacitor electrodes. J Power Sour 2010;195(2):667–73.
[40] Hulicova D, Kodama M, Hatori H. Electrochemical performance of nitrogen-enriched carbons in aqueous and non-aqueous supercapacitors. Chem Mater 2006;18(9):2318–26.
[41] Hulicova D, Yamashita J, Soneda Y, Hatori H, Kodama M. Supercapacitors prepared from melamine-based carbon. Chem Mater 2005;17(5):1241–7.
[42] Perez-Cadenas M, Moreno-Castilla C, Carrasco-Marin F, Perez-Cadenas AF. Surface chemistry, porous texture, and morphology of N-doped carbon xerogels. Langmuir 2008;25(1):466–70.
[43] Wang Y, Su F, Lee JY, Zhao XS. Crystalline carbon hollow spheres, crystalline carbon-SnO_2 hollow spheres, and crystalline SnO_2 hollow spheres: synthesis and performance in reversible Li-ion storage. Chem Mater 2006;18(5):1347–53.
[44] Su F, Zhao XS, Wang Y, Zeng J, Zhou Z, Lee JY. Synthesis of graphitic ordered macroporous carbon with a three-dimensional interconnected pore structure for electrochemical applications. J Phys Chem B 2005;109(43):20200–6.
[45] Zhao C, Wang W, Yu Z, Zhang H, Wang A, Yang Y. Nano-$CaCO_3$ as template for preparation of disordered large mesoporous carbon with hierarchical porosities. J Mater Chem 2010:976–80.
[46] Gierszal KP, Jaroniec M. Carbons with extremely large volume of uniform mesopores synthesized by carbonization of phenolic resin film formed on colloidal silica template. J Am Chem Soc 2006;128(31):10026–7.
[47] White RJ, Tauer K, Antonietti M, Titirici M-M. Functional hollow carbon nanospheres by latex templating. J Am Chem Soc 2010;132(49):17360–3.
[48] Oya A, Otani S. Effects of particle size of calcium and calcium compounds on catalytic graphitization of phenolic resin carbon. Carbon 1979;17(2):125–9.
[49] Tan H, Wang X, Wang C, Xu T. Characteristics of HCN removal using CaO at high temperatures. Energy & Fuels 2009;23(3):1545–50.
[50] Ohtsuka Y, Xu C, Kong D, Tsubouchi N. High catalytic performances of low-rank coal chars in ammonia decomposition at high temperatures. Fuel Chem Div Prep 2003;48(1):304–5.
[51] Pickles CA, Toguri JM. Thermodynamic analysis of the Ca–C–N system. High Temp Mater Process 2004;23(5–6):405–18.
[52] Boehm HP. Formation of well-crystallized graphite in the calcium cyanamide process. Carbon 1978;16(5):385–7.
[53] Schaefer ZL, Gross ML, Hickner MA, Schaak RE. Uniform hollow carbon shells: nanostructured graphitic supports for improved oxygen-reduction catalysis. Angew Chem Int Ed 2010;49(39):7045–8.